Computational Evaluation of the Neural Activity Model of Retinotopic Map Formation

UNIVERSITY OF CAMBRIDGE

Name: George Baxter

Supervisor: Dr Stephen Eglen

Word Count: 5993

Abstract

A computational model was constructed in the Python™ and Cython programming languages and used to evaluate Willshaw and Malsburg's neural activity theory of topographically organised network development. The investigation focuses on the development of retinotopic maps in the optic tectum of fish and amphibians. This study demonstrates that the neural activity model is able to successfully explain the systems-matching results observed in surgical mismatch experiments and that the model is robust to different patterns of retinal activity. Eight different types of retinal activity pattern are investigated, and a novel function is developed to allow quantitative assessment of the retinotopic maps produced by the model.

*

Contents

Abbreviations

AP - Activity pattern

MD – Manhattan distance

PM – Polarity marker

Introduction

A topographically organised neural map is the ordered projection of neighbouring cells in one neural sheet to neighbouring cells in another. Topographic maps typically project from a sensory surface and convey information to structures within the CNS. Notable examples include: a two-dimensional map of the retina on the surface of the striate cortex in higher vertebrates (Talbot and Marshall, 1941) and on the surface of the superior colliculus in both higher and lower vertebrates (termed the optic tectum in lower vertebrates) (Apter, 1945; Cooper et al., 1953; Gaze, 1958), the two-dimensional somatotopic organisation of the somatosensory cortex (Penfield and Boldrey, 1937) and motor cortex (Woolsey, 1952), as well as the conservation of the one-dimensional tonotopic organisation of the cochlea in the early (pre-cortex) auditory pathway (Rose et al., 1959). This study investigates *in silico* how topographically organised neural networks form, focussing on the development of retinotopic maps in the tectum of fish and amphibians. These maps form as the consequence of the topologically ordered projection of retinal neurons to the contralateral tectum (Gaze et al., 1970), and is an area of great experimental research.

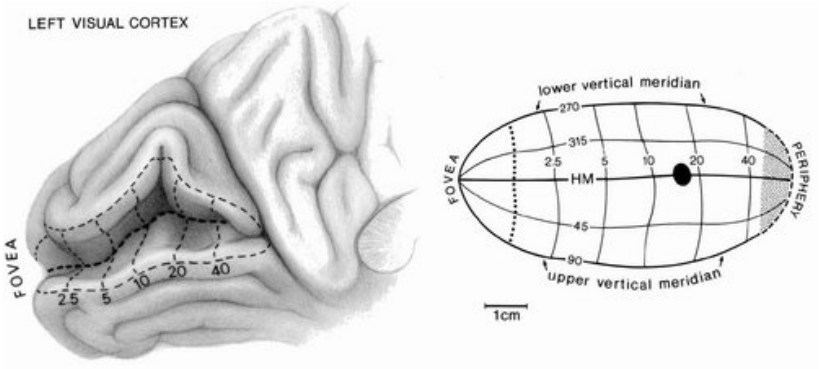

Figure 1: Left: Modern day estimate of the representation of the visual field on the surface of human occipital cortex. Right: representation of visual field coordinates as they would appear on the cortex if completely unfolded and flattened. Numbers show either meridional angle or eccentricity in degrees. The dark circle is the blind spot; HM = horizontal meridian. Image reproduced from www.scholarpedia.org/article/Visual_map

The long-term goal of studying topographic map formation is the hope that understanding the mechanisms underling development will give crucial insights into how to regenerate these networks after injury.

Theories of Retinotopic Map Formation

The principle point of research is into how axonal projections from the presynaptic sheet (the retina in this case) form ordered, topographic connections with the postsynaptic sheet (the tectum). Research in this field has historically focussed on fish and amphibians because it is possible to perform surgical manipulations on the retina and tectum, and then investigate (histologically and electrophysiologically) the distribution of retinal projections to the tectum produced after the optic nerve redevelops (Gaze et al., 1970). A key assumption of the research is that the mechanisms responsible for organising nerve connections during embryological development are also responsible for organisation during regeneration.

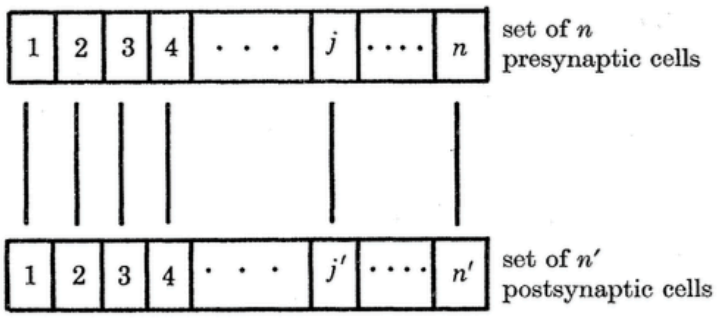

Figure 2: The problem under discussion. How does presynaptic axon j contact the appropriate post synaptic cell, j'? Image replicated from Prestige and Willshaw, 1975.

The original theory of the mechanism underlying this process is Sperry's theory of neuronal specificity (Sperry, 1943, 1963):

(1) During development, retinal neurons undergo a differentiation process and each develop a unique chemical marker (e.g. an extracellular or transmembrane protein).

(2) The tectal neurons undergo a similar process.

(3) A ‘matching’ process takes place; retinal and tectal neurons with corresponding markers form strong synaptic connections.

This is a direct-matching theory, as each presynaptic neuron has a defined affinity for each postsynaptic neuron, determined by the degree of similarity between their respective markers. The highest affinity is for the postsynaptic neuron whose marker most closely resembles its own (Prestige and Willshaw, 1975). However the results observed after surgical mismatch experiments — in which a section of either the retina, the tectum, or both is removed — cannot be explained by direct-matching theories (Prestige and Willshaw, 1975). The results indicate that ‘systems-matching’ is taking place — the whole of the retina (or the part that remains after surgery) maps in a continuous fashion to the whole of the tectum (or the part that remains after surgery) in the correct orientation (Gaze and Keating, 1972). As a consequence new theories were developed to explain the observed systems-matching including the marker induction hypothesis (Willshaw and Malsburg, 1979) and the neural activity model (Willshaw and Malsburg, 1976). This study focuses on the latter.

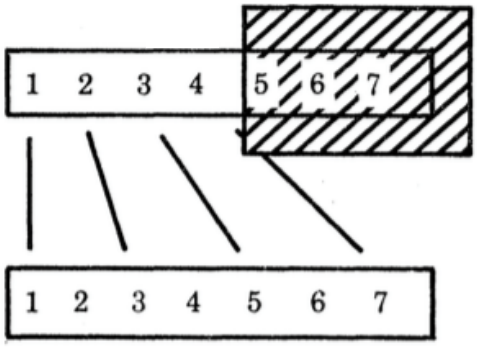

Figure 3: Diagram of systems-matching in post mismatch surgery amphibians. Half the retina has been ablated and the remaining axons spread to synapse with the whole tectum. Image replicated from Prestige and Willshaw, 1975.

Neural Activity Model

This model hinges around the principle that prospective partners of neighbouring presynaptic cells are neighbours in the postsynaptic sheet. If an optimisation process can ensure that all pairs of neighbouring retinal neurons form synaptic connections with neighbouring tectal neurons, the resulting map will be topographically

organised. The key requirement is that the distance between retinal neurons is encoded in the model, allowing the notion of neighbours to be established. In the neural activity model this is achieved by ensuring that electrical activity in adjacent cells in the retinal and tectal sheets is correlated. Correlation in the retinal sheet is ensured by assuming that random clusters of adjacent presynaptic cells are activated during development. Correlation in the tectal sheet is facilitated by local connections resulting in short-range excitation and long-range inhibition — this network schematic is often referred to as Mexican-hat connectivity and is thought to be crucial to path integration in the hippocampus and entorhinal cortex (McNaughton et al., 2006; Moser et al., 2014). Using this network schematic it can be intuited that a cluster of adjacent neurons in the post-synaptic sheet will end up firing more than the rest of the sheet, i.e. correlated activity between adjacent neurons is achieved. By having the geometrical proximity of neurons in the pre- and postsynaptic sheets encoded by the correlations in their electrical activity, Hebbian plasticity (Hebb, 1949) will strengthen the connections between neighbouring neurons in the retina and neighbouring neurons in the tectum, therefore resulting in continuous mapping and network self-organisation (Willshaw and Malsburg, 1976).

Aims of this Study

The aim of this study is to construct a model of, and computationally evaluate, the neural activity theory. The investigation will focus on whether the neural activity model can explain observed systems matching results, and whether the model is robust to various different patterns of retinal activity. In this study the retinal and tectal sheets modelled are expanded to 10x10 and eight different types of retinal APs — with varying degrees of correlation — are investigated. A method of quantitatively assessing the quality of the retinotopic maps produced by the model is devised, allowing statistical analysis.

Materials and Methods

A computational model based on the neural activity theory of topographic network formation was constructed in the Python™ programming language (v.2.7.12). The Scipy (v.0.19.0) and Numpy (v.1.12.0) libraries were used in the model as they are optimised for numerical calculations. Novel functions were converted into a Cython (v.0.24) library and compiled into C, resulting in a c.6x speed-up of the model. This reduced computational constraints, therefore facilitating modelling of larger retinotopic maps. Plotting of the retinotopic maps was conducted using Seaborn (v.0.7.1) and Matplotlib (v.2.0.0).

The Python™ and Cython scripts can be found in the following GitHub™ repository: **https://github.com/geobax/correlated_activity_76**
These scripts are heavily annotated; queries regarding the implementation or functioning of the model should be addressed by referring to the below section 'Constructing the Model' and to the scripts in the GitHub™ repository.

Constructing the Model

The model was predominantly constructed based on the appendix of Willshaw and Malsburg, 1976, and is replicated here in full (Appendix - Figures 33 and 34). I have broken down the aforementioned appendix into discrete sections and will explain how each is recreated in the model. Fig.4 gives a general overview of how the model works.

INITIALISATION

- Create matrix of strengths of synaptic connections between retinal and tectal neurons
- Bias the connections between polarity marker neurons

DEVELOPMENT

(1) Create retinal activity
(2) Induce tectal activity
(3) Calculate effects of tectal lateral connectivity
(4) Hebbian update
(5) Synaptic normalisation

Steps 1-5 are iterated over a predefined number of times.

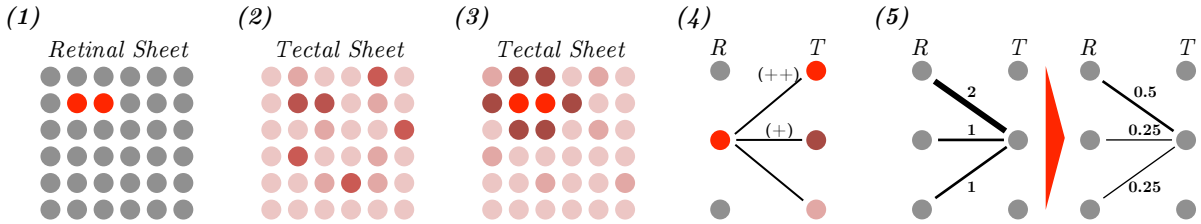

ANALYSIS

- Centres of the tectal neuron receptive fields are calculated and plotted
- Quality of the resulting retinotopic map is calculated
- INITIALISATION and DEVELOPMENT are performed ten times, producing ten individual retinotopic maps
    - Mean and standard deviation in quality is calculated

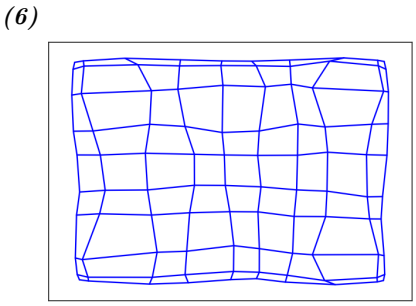

QUALITY = 0.965
GROUP MEAN = 0.959 ± 0.007

Figure 4: Model overview. Figure describes in brief how the computational model functions. Sub-images 1-5 are diagrammatic representations of Development steps 1-5. (1) 2 adjacent retinal neurons are activated. (2) The tectal neurons connected to these retinal neurons are activated; their activity is proportional to retino-tectal synaptic strength, which is initially random. Activity is indicated by the intensity of red. (3) Tectal interactions are considered; a stable centre of activity is established — note this could form anywhere in the tectal sheet, here it is shown in a corresponding location to the active retinal neurons for the sake of simplicity. (4) Hebbian plasticity increases the synaptic strength between the active retinal neurons and tectal neurons firing strongly. (5) Synaptic strengths are then normalised such that each tectal neuron has a fixed total synaptic strength to the retinal sheet. This example shows total synaptic strength being normalised to 1. Sub-image (6) shows the output of the model: a plot of the centres of the tectal receptive fields, alongside the quality of the individual map and the mean and standard deviation of the group of 10 that were produced.

SECTION 1 - INTIALISATION

The strength of the synaptic connection between cell i in a sheet of M presynaptic cells and cell j in a sheet of N postsynaptic cells is specified by the entry s_{ij} in the $M \times N$ matrix s. The activity H_j^* in postsynaptic cell j is determined by its mem-

Figure 5: Appendix — Section 1.a

For the initial values in the matrix s a set of MN random numbers were first chosen from a normal distribution of mean 2.50 and standard deviation 0.14. The

Figure 6: Appendix — Section 1.b

The model generates a matrix ('s') containing the initial strengths of synaptic connections between each retinal and tectal neuron. The retinal neurons are represented by the x-dimension of 's', and the tectal neurons by the y-dimension; the strength of a particular retino-tectal synapse is given by the value in the matrix corresponding to the intersection between the retinal neuron's column and the tectal neuron's row. The initial values are sampled from a normal distribution with a mean of 2.5 and standard deviation of 0.14, the same values used by Willshaw and Malsburg.

SECTION 2 – MODELLING DIFFERENTIAL EQUATIONS

$M \times N$ matrix s. The activity H_j^* in postsynaptic cell j is determined by its membrane depolarization H_j, and is calculated according to a linear threshold model of a nerve cell (Malsburg 1973). At time t, cell j is deemed to fire if its depolarization exceeds a fixed threshold value θ. Its activity $H_j^*(t)$ is defined as

$$H_j^*(t) = \begin{cases} H_j(t) - \theta & \text{if} \quad H_j(t) > \theta, \\ 0 & \text{otherwise.} \end{cases}$$

Figure 7: Appendix — Section 2.a

The model uses a linear threshold function to convert tectal neuron membrane depolarisation to a post-threshold activity. The threshold value ('theta') is set at 10.0, the same value used by Willshaw and Malsburg.

To calculate the membrane depolarization we assume that its rate of change $\partial H_j/\partial t$ is proportional to the sum of the excitatory effects of active presynaptic cells, the excitation and inhibition supplied by nearby active postsynaptic cells and a decay term due to losses in the membrane itself. It is helpful to define the quantities $A_i^*(t)$, e_{kj} and i_{kj}. The variable $A_i^*(t)$, used to describe the state of the presynaptic cells, has value 1 if cell i is active at time t and 0 otherwise. The time independent parameters e_{kj} and i_{kj} specify the short range excitation and inhibition exerted by postsynaptic cell k on postsynaptic cell j.

We can then write a set of N coupled equations.

$$\frac{\partial H_j(t)}{\partial t}+\alpha H_j(t) = \sum_i A_i^*(t)\, s_{ij}(t)+\sum_k H_k^*(t)\, e_{kj}-\sum_k H_k^*(t)\, i_{kj} \quad \text{for} \quad j = 1,2,3,\ldots, N.$$

The first sum represents the contributions from the presynaptic cells; the other two are the excitatory and inhibitory contributions from the postsynaptic cells. The parameter α is the membrane time constant. To ensure that cells which do not

Figure 8: Appendix — Section 2.b

The model calculates the membrane depolarisation of tectal neurons using Euler integration to solve the above differential equation. The results of short-range excitatory and long-range inhibitory interactions within the tectal sheet are solved using a convolution function. Convolution functions are typically used in signal and image processing to combine information from different cells of a matrix, e.g. the mixing of colours between neighbouring pixels in order to blur an image. The coefficients of short and long-range interactions (based on post-threshold activities) within the tectal sheet are modelled in the convolution function as the same as those in Willshaw and Malsburg (0.05 and 0.025 for the excitatory interactions between neurons that are separated by 1 Manhattan distance (MD) and 2 MD respectively, and 0.06 for the inhibitory interactions between neurons that are separated by 3 MD. The model uses a membrane time constant ('alpha') of 0.5, the same used by Wilshaw and Malsburg.

Section 3 – Polarity Markers

normally distributed about a positive mean. The numbers are then adjusted to give synapses between polarity marker cells above-average strengths. The following

Figure 9: Appendix — Section 3

Willshaw and Malsburg used the concept of polarity markers (PMs) to ensure that the tectal retinotopic maps preserve the orientation of the retina. PMs are a group of retinal neurons that are pre-disposed to forming strong synaptic connections with a group of tectal neurons; the specificity of these connections encodes the orientation of the tectal map (Fig.10). The option for three different 'styles' of PM were built into the model. The first two are analogous to those used by Willshaw and Malsburg.

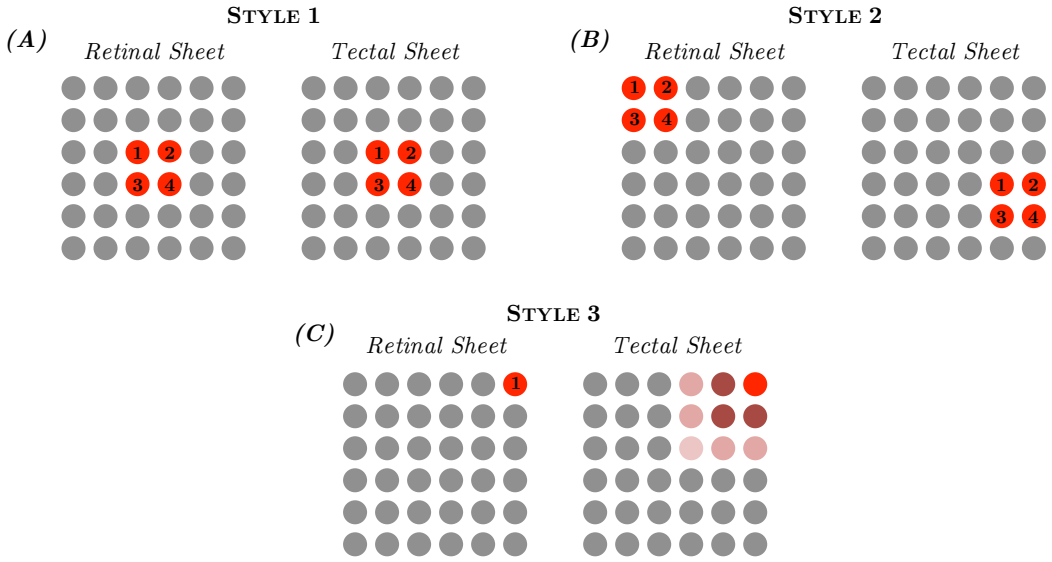

Figure 10: Image showing the three different styles of polarity markers that can be implemented using the model. In all three cases the grid of dots represent individual neurons in the retinal and tectal sheets; red dots represent neurons involved in the construction of the polarity markers, grey dots represent the other neurons in the sheets that are not relevant to a discussion regarding polarity markers. (A) Style 1. The synaptic strength between the comparatively labelled neurons in the retinal and tectal sheets is increased, therefore encoding the polarity of the retinal sheet in the tectal representation of the retina. The central position of these polarity markers leads to reliable nucleation of the retinotopic map. (B) Style 2. The orientation of the retinal sheet is encoded in the same way as style 1, however the position of the polarity markers in the retinal and tectal sheets is chosen at random. This often leads to nucleation starting off-centre, however correlated activity in the retinal sheet is usually sufficient to overcome this (Results – Fig.23). (C) Style 3. The retinal neuron labelled 1 is connected more strongly to those red neurons in the tectal sheet — the more intense the shade of red, the stronger the connection to retinal neuron 1. This process is conducted for every retinal neuron (only one is showed here for simplicity), therefore laying down an embryonic map of the retina in the tectum by encoding the relative positions of every neuron, before correlated activity in the retinal sheet refines and further specifies the map. The synaptic connection strength between a retinal neuron and neurons in the tectal sheet is increased in a graded way for tectal neurons up to half the maximum distance away (e.g. half the diagonal of the tectal sheet) from the relative position of the retinal neuron in question; the strength of connections to those tectal neurons further away is not altered.

In the **first style** PMs on the retinal and tectal sheets are set as the four most central neurons (Fig.10a), predisposing them to pair strongly with their correct counterparts in the tectal sheet.

The **second style** selects a random 2x2 square of retinal neurons and a random 2x2 square of tectal neurons to act as the PMs (Fig.10b). This introduces strong erroneous connections into the initial map, but results from the model show that this can be overcome and high quality maps can still successfully form (RESULTS — Fig.23).

The **third style** implements graded PMs (Fig.10c) (Goodhill, 1993). The strength of synaptic connections between retinal and tectal neurons is increased based on their relative positions in the sheets; the closer the relative positions the more synaptic strength is increased. This is similar to using chemical markers to lay down an initial map, before correlated activity takes over. The strength of synaptic connections between the retinal and tectal neurons selected as PMs is increased five-fold in styles 1 and 2, and increased in a graded way up to five-fold in style 3 (see Fig.10 caption for more detail).

PMs also act to prevent the developing retinotopic map from getting caught in a local optimum. If this were to happen the map could only further improve via partial destruction and reformation; this cannot be carried out by the microscopic mechanism of the neural activity model. Local optima could occur if map formation began at more than one centre, leading to the formation of two (or more) incompatible part-maps. PMs avoid this by predisposing the map to begin to form around the initial strong connections between the PMs in the retinal and tectal sheets — this is most apparent in polarity marker styles 1 and 2, where the polarity markers act as a 'nucleation-centre' for map development. The non-central nucleation centre in polarity marker style 2 is inherently less stable than the central nucleation afforded by style 1 as there is more scope for errant connections to be strengthened further away from the nucleation centre, and the nucleation centre itself is required to 'drift' to it's correct location. This leads to more variable and lower average

quality maps, however high quality maps can still form (Fig.23). In PM style 3 the issue of part-map formation is overcome by encoding the correct relative position of the tectal neurons at the beginning of the process — this initial bias is then hard to overcome, evidenced by the increased quality of maps produced (Fig.24).

Section 4 – Map Development

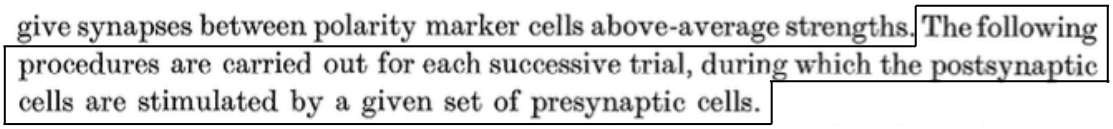
give synapses between polarity marker cells above-average strengths. The following procedures are carried out for each successive trial, during which the postsynaptic cells are stimulated by a given set of presynaptic cells.

Figure 11: Appendix — Section 4.a

The model is constructed such that it constitutes a single major loop. This loop incorporates each of the following steps:

Step 1 — Activating the retinal sheet

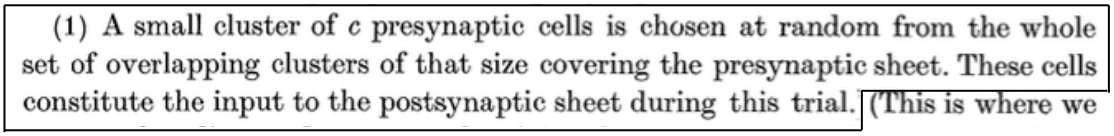
(1) A small cluster of c presynaptic cells is chosen at random from the whole set of overlapping clusters of that size covering the presynaptic sheet. These cells constitute the input to the postsynaptic sheet during this trial. (This is where we

Figure 12: Appendix — Section 4.b

The first stage of each iteration is the activation of a group of retinal neurons. Willshaw and Malsburg tested two different types of retinal activity patterns:

(1) Randomly selected pair of adjacent retinal neurons (Fig.13a)

(2) Two randomly selected pairs (Fig.13b).

Little is known about the actual retinal APs that occur during the development of retino-tectal projections (Arroyo and Feller, 2016). In order to investigate how robust the theory of neural activity is, six novel APs were devised, with varying levels of correlation.

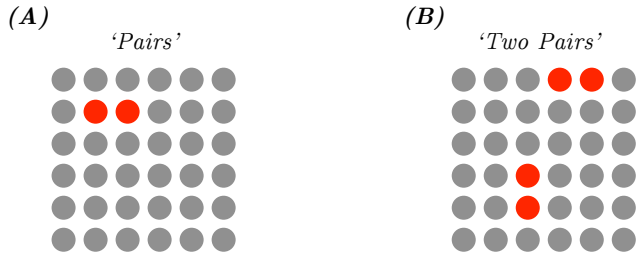

Figure 13: Original activation patterns from Willshaw and Malsburg, 1976. The matrix of dots represents the retinal sheet; each dot represents an individual retinal neuron. Red dots indicate neurons that are activated by the activation pattern in question. (A) A representation of the activation of a single pair of retinal neurons. (B) A representation of the second style of activation pattern, the activation of two independently selected random pairs of retinal neurons.

These are as follows:

(1) 'Squares' — randomly selected 2x2 squares

(2) 'Singles' — randomly selected single retinal neuron

(3) 'Two singles' — two randomly selected single retinal neurons

(4) 'Sweep' — here the retinal sheet is 'swept' across. This is modelled as sequential activation of first the columns of retinal neurons (from left to right), and then the rows (from top to bottom)

(5) 'Ocular dominance' — the left and right halves of the retinal sheet are alternately activated

(6) 'Strobe' — activation of the entire retinal sheet

See Fig.15 for diagrammatic representations of these novel retinal APs.

In the case of the original APs and novel APs 1-3, the model operates by selecting an arbitrary retinal neuron using random x and y coordinate within the boundaries of the retinal sheet. Additional retinal neurons required for the AP are then selected via random choice between the appropriate combinations of x and y coordinates. For 'two pairs' and 'two singles' the possibility of selecting the same retinal neurons in the two sets is omitted. The x and y coordinates for each selected retinal neuron are converted into an integer uniquely identifying that neuron's position within the retinal sheet using the following equation (Fig.16):

$$\mathbf{N} = \boldsymbol{y} \mathbf{*} \mathbf{XR} + \boldsymbol{x}$$

APs 4-6 are modelled differently. For 'sweep' pattern the retinal row/column to be activated is selected based on remainder division of the current iteration number by the total number of rows and columns. In the ocular dominance activity pattern remainder division of the loop number by 2 determines which half of the retinal sheet is activated — e.g. a remainder of 0 activates the left half, whilst a remainder of 1 activates the right half. The strobe pattern is simply modelled such that the entire retinal sheet is activated.

STEP 2 — ACTIVATING THE TECTAL SHEET

> (2) For each of the N postsynaptic cells a stationary solution for its membrane depolarization is found by iterating the set of coupled equations until the mean change in depolarization per unit of time becomes less than 0.5%.

Figure 14: Appendix — Section 4.c

Tectal neuron depolarisation is calculated using Euler integration of the differential equation in Fig.8. This is achieved as follows:

(1) Initial depolarisation of the tectal neurons due to retinal activation is calculated first. For each tectal neuron this is given by the sum of the strengths of its synaptic connections with the active retinal neurons (Fig.8). The columns of 's' give the strength of the synaptic connections between the retinal neuron that corresponds to said column (as given by the unique retinal identification number — see Fig.16) and every tectal neuron (each of which is identified by a unique tectal identification number, calculated in the same way as their retinal counterparts, and corresponds to the rows of 's'). By summing (row-wise) the columns of 's' that correspond to the activated retinal neurons the model calculates the initial depolarisation of each tectal neuron.

(2) The post-threshold activity of each tectal neuron is calculated using the threshold function.

(3) The post-threshold activities are used to calculate the result of the interactions within the tectal sheet.

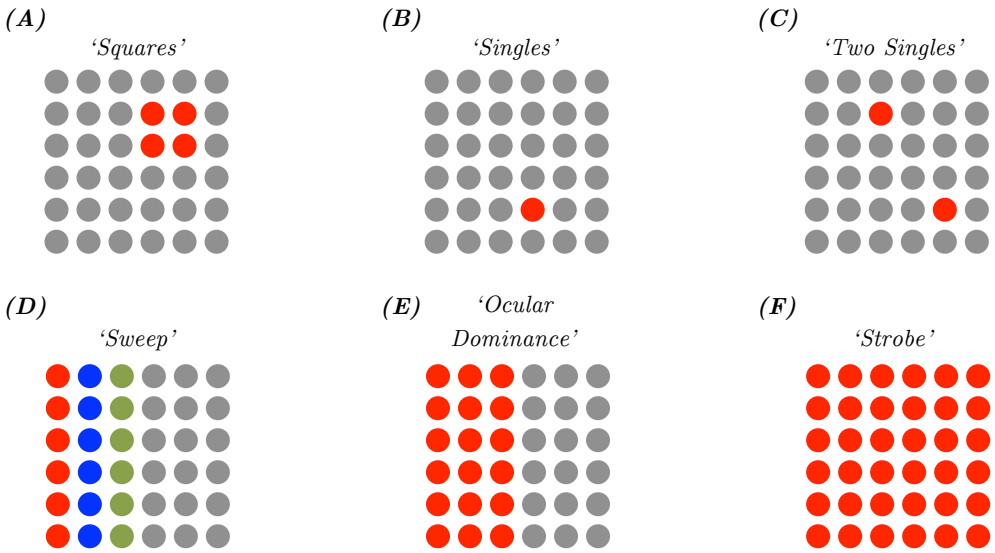

Figure 15: Novel retinal activation patterns. The matrix of dots represents the retinal sheet; each dot represents an individual retinal neuron. Coloured dots indicate neurons that are activated by the activation pattern in question. (A) 'Squares' activation pattern; a 2x2 square of retinal neurons is randomly selected and activated. (B) 'Singles' activation pattern; a single retinal neuron is selected and activated. (C) 'Two Singles' activation pattern. (D) 'Sweep' style activation pattern. The retinal sheet is 'swept' across, with each column activated in turn (from left to right), followed by the sequential activation of each row (from top to bottom). In this representation the red neurons represent those activated during the first loop, those in blue the second loop, and those in green the third loop. In this example, the activity pattern would repeat every 12 loops. (E) 'Ocular dominance' style retinal activation pattern. The left and right halves of the retinal sheet are alternately activated. (F) 'Strobe' activation pattern. Here the entire retinal sheet is activated each loop.

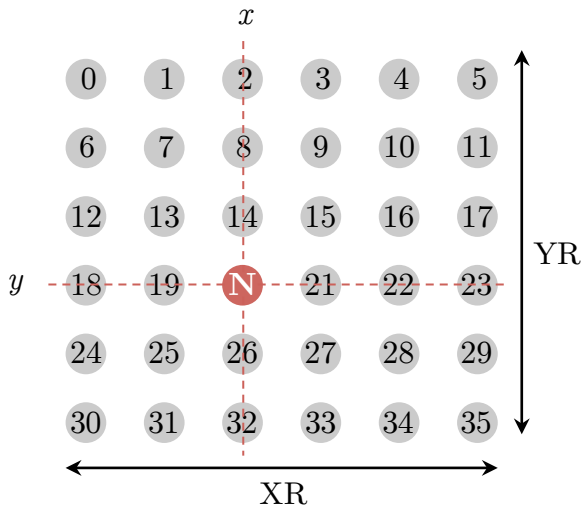

Figure 16: Unique retinal neuron numbers. The figure shows a 6x6 retinal sheet. Each grey dot represents a single retinal neuron; the overlaid numbers correspond to the unique number that identifies the position of each retinal neuron within the sheet (note that Python™ utilises index base 0). 'XR' and 'YR' are the x- and y- dimensions of the retinal sheet respectively. The unique number for retinal neuron 'N' can be calculated from its it's x and y coordinates (note: base 0) using the following equation: N = y * XR + x.

(4) The depolarisation of each tectal neuron is then multiplied by the membrane decay constant.

Steps 1-4 are then iterated over until the tectal sheet converges; convergence is defined as less than 0.5% deviation in the mean depolarisation of the tectal sheet between successive iterations.

STEP 3 — MODIFYING SYNAPTIC STRENGTHS

(3) Only those synapses between cells firing sufficiently strongly are strengthened. The increase in strength Δs_{ij} of synapse s_{ij} is given by

$$\Delta s_{ij} = h A_i^* H_j^*$$

provided that H_j^*, as calculated in step 2, exceeds the modification threshold ϵ, and where the constant h sets the speed of organization.

Figure 17: Appendix — Section 4.d

After convergence the post-threshold depolarisation of each tectal neuron is used to influence the strength of the synaptic connection between the activated retinal neurons and the tectal neuron in question (Hebbian plasticity). Synaptic strengths are only increased if tectal neuron post-threshold depolarisation exceeds the modification threshold; if so the synaptic strength is increased in proportion to the post-threshold depolarisation. The constant of proportionality, 'h', sets the speed of organisation. Willshaw and Malsburg used h=0.016 for the single pairs activity pattern; the new model typically requires values an order of magnitude smaller to produce reliable maps. This is likely because the maps generated in this study are larger, therefore there is more scope for the formation of erroneous connections in the early stages of map development. A lower 'h' reduces the magnitude of erroneous connections, making it easier for correct connections to overcome them. The threshold for tectal neuron firing and the threshold for synaptic modification are scaled with the number of retinal neurons activated by the activity pattern.

Step 4 — Synaptic Normalisation

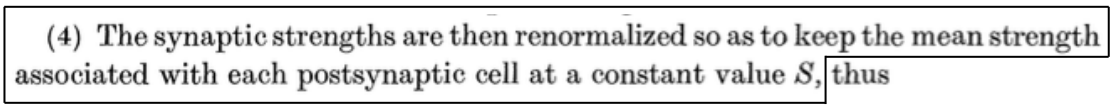
(4) The synaptic strengths are then renormalized so as to keep the mean strength associated with each postsynaptic cell at a constant value S, thus

Figure 18: Appendix — Section 4.e

From Step 3 it is apparent that the model only has a mechanism to increase synapse strengths. To prevent synaptic strengths spiralling to implausibly high values, a normalisation stage is required. This ensures that the mean strength of synaptic connections associated with each cell in the tectal sheet remains at a fixed value, 'S'. The model implements this by calculating the mean of each row of 's' (e.g. the mean strength of synaptic connections with each tectal neuron), dividing the individual values in each row by this mean strength, and then multiplying them by 'S'. The same value of 'S' is used in the model as was used by Willshaw and Malsburg, 'S' = 2.5.

Steps 1-4 are then iterated over multiple times. Willshaw and Malsburg typically iterated 10,000 times. In this study 500,000 iterations are typically used. The reason for this is two-fold: the retinal sheets modelled are larger, therefore more iterations are required in order to activate each retinal neuron a similar number of times, and secondly, the value of 'h' used is lower, hence more iterations are required in order for a retinotopic map to form fully. Unless stated otherwise it can be assumed that:

- 'h' = 0.0016
- the dimensions of the retinal and tectal sheets are 10x10
- 500,000 iterations are used

Qualitative and Quantitative Evaluation of Model Output

In Willshaw and Malsburg, 1976, model outputs were only evaluated qualitatively via the plotting of the resulting retinotopic maps. This study follows the original paper by producing charts of a similar style. However, a Python™ function was produced

that assigns the retinotopic maps a 'quality', therefore also allowing quantitative assessment.

Chart plotting

After iterating steps 1-4 of the, the final synaptic weight matrix is used to calculate the coordinates of the 'centre of mass' of the synaptic connections between each tectal neuron and the retinal sheet. This corresponds to the centre of each tectal neuron's receptive field. These centre of mass coordinates are then plotted using the Seaborn extension of Matplotlib (Fig.19).

Quality function

Maps produced by the model are assigned a 'quality', determined by comparing the final position of the centre of mass of each tectal neuron to their ideal position. The displacements are calculated as a Pythagorean distance, and normalised to the maximum possible displacement — the diagonal of the tectal sheet. These normalised displacements are summed and divided by the number of tectal neurons. The final quality of a map is given by 1 minus the normalised displacement, yielding a value between 0-1. The higher the quality, the smaller the average displacement, per tectal neuron. For each set of input parameters the model is run ten times, generating a batch of retinotopic maps; the mean and standard deviation of the quality of these maps is calculated (Fig.19).

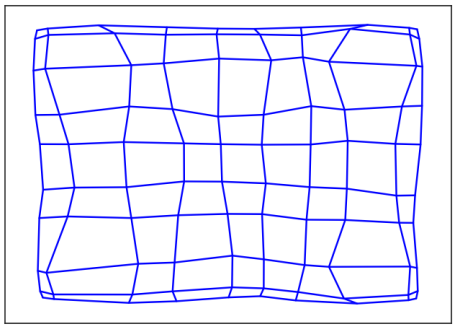

Quality = 0.965

group mean = 0.959 ± 0.007

Figure 19: Example plot. The black line around the perimeter of the plot denotes the perimeter of the retinal sheet. The dimensions of the plot are normalised to the dimensions of the retinal sheet. Points associated with neighbouring tectal cells are joined by straight lines. This plot shows the result of a 10x10 retinal sheet plotting to a 10x10 tectal sheet. Polarity marker style 1 and the 'pairs' activity pattern were used.

RESULTS

This section documents the output of the computational model. It is divided into subsections that demonstrate how the model was used to evaluate the neural activity model.

VERIFYING MODEL FUNCTION

In order to do novel research it must be demonstrated that the model is functionally robust. This is achieved by investigating whether the model can successfully reproduce results from Willshaw and Malsburg, 1976.

SYSTEMS-MATCHING AND 'PAIRS' ACTIVITY PATTERN

The model can produce high quality retinotopic maps between retinal and tectal sheets of different sizes (Fig.20), therefore demonstrating systems matching, the key criteria of assessing the success / viability of the neural activity model in network self-organisation. See Willshaw and Malsburg, 1976 – Figure 3 for the original plots.

POLARITY MARKER STYLES

As discussed in MATERIALS AND METHODS, the model includes the option for three different styles of PM. In order to understand how these styles differ from one another it is useful to see how they influence the embryonic retinotopic maps, and the impact on the final retinotopic maps produced. Figures 21-24 show a no PM style and PM styles 1-3 respectively, after 0 and 500,000 iterations. The initial bias introduced by styles 1 and 2 is subtle, whereas style 3 introduces a template for the final retinotopic map. More detail on all of the different PM styles can be found in METHODS AND MATERIALS. Retinotopic maps fail to develop in the absence of polarity markers (Fig.21); without the increase in synaptic strengths afforded by PMs, the retinal drive to the tectal sheet is insufficient to cause tectal neurons to

fire. Given more time, Willshaw and Malsburg's claim that retinotopic maps are prone to rotation in the absence of PMs could be investigated by lowering the thresholds for neural firing and synaptic modification. The qualities of the embryonic maps (Figures 21A, 22A, 23A and 24A) give a baseline with which to compare final retinotopic maps. Initial maps produced using the 'no polarity marker' style (Fig.21A) have a quality greater than 0 (0.730 ± 0.000). A quality of 0 represents a map where every tectal neuron's centre of mass is the maximum possible displacement away from its ideal location; Fig.21A is an unformed retinotopic map, as opposed to an ill-formed retinotopic map. PM style 2 (Fig.23) is used to show that PMs are only required to set the orientation of the final map, as opposed to introduce initial strong connections between corresponding neurons in the pre- and post-synaptic neural sheets. The low average quality (0.750 ± 0.085) of the maps it generates is likely a function of too few iterations. Theoretically higher iteration numbers could generate consistently higher quality maps, but due to temporal and computational constraints this has not been tested. For the investigations into novel APs, PM styles 1 and 3 are used. Some APs require the initial bias of PM style 3 in order to form high quality retinotopic maps.

Original Activity Patterns

Willshaw and Malsburg tested their model on two activity patterns (APs): 'pairs' and 'two pairs' (See Fig.12). The model successfully reproduces the results for the 'pairs' pattern (Fig.20A), however Willshaw and Malsburg didn't publish plots for the 'two pairs' pattern, therefore no comparison can be made. 'Two pairs' maps appear well formed, but are under-sized (Fig.25). The use of two separate pairs of active retinal neurons means the degree of correlation in retinal activity varies based on the positioning of these pairs. If the pairs are adjacent, then retinal activity is highly correlated and the synapses strengthened as a consequence will be between neighbours. Correlated activity strengthening connections to neighbouring tectal neurons explains the correct relative positions of their centres of mass, and by increasing the strength of connections between each tectal neuron and the entire

retinal sheet (on average, across many iterations), the uncorrelated activity explains the small size of the maps formed.

Novel Activity Patterns

New retinal APs were devised to test whether the neural activity theory is robust to different patterns of retinal activity, and how the degree of correlation of retinal activity affects map development. These novel retinal APs are:

(1) 'Squares'

(2) 'Singles'

(3) 'Two singles'

(4) 'Sweep'

(5) 'Ocular dominance'

(6) 'Strobe'

See Materials and Methods for further detail.

'Squares'

The 'squares' AP is more highly correlated than the 'pairs' AP — four retinal neurons in close proximity simultaneously active, as opposed to two. Theoretically this gives more scope for errant connections to be strengthened, as the tectal sheet cannot distinguish between the four active retinal neurons. This is known as over-correlated activity. In the case of the 'squares' AP, over-correlation is not a major issue; high quality maps form with both PM style 1 and 3 (0.898 ± 0.026 and 0.953 ± 0.001 respectively) (Fig.26). When using PM style 1, the corner tectal neurons have a tendency to not develop specific connections, with their centre of mass remaining in the centre of the retinal sheet (Fig.26A). This is because the corner retinal neurons can only be activated as part of one square of retinal neurons, therefore are 4x less likely to be activated than central retinal neurons, so their synapses specify less. This doesn't occur using style 3, where the corners already have a preliminary specificity. Over-correlation in the 'squares' AP means that outer

layer of retinal neurons cannot be distinguished from the layer inside — as they are always active at the same time — explaining the failure of the outer layer of tectal neurons to separate from the penultimate layer.

'SINGLES'

The 'singles' AP has no correlation in retinal activity, hence *a priori* the network is not expected to self-organise (Fig.27).

'TWO SINGLES'

The 'two singles' AP involves activating two independently selected random single retinal neurons. Much like the 'two pairs' activity pattern, 'two singles' results in varying levels of correlation in retinal activity. Using PM style 1, maps fail to develop (Fig.28A); the number of iterations used was too few for the random occurrences of correlated activity to be sufficient to form the map. Given more time, number of iterations could be increased to test for further development. Retinotopic maps do form using PM style 3 (Fig.28B); the initial embryonic map afforded by style 3 allows the low incidences of random correlated activity to be sufficient for the map to develop.

'SWEEP'

Successive rows and columns of retinal neurons are activated (see METHODS AND MATERIALS). This AP is designed to simulate waves of activity sweeping across the retinal sheet. Maps fail to develop with PM style 1 (Fig.29). The activity in each row and column is over-correlated; the tectal sheet is unable to differentiate between the neurons active at any one time — within a column the mean synaptic centre of mass of the tectal neurons will tend towards the centre of the column, whilst in a row, the centre of mass will tend towards the centre of the row. Because every tectal neuron is active as part of both a row and a column, the synaptic centres of mass tend towards

the centre of the retinal sheet, hence the maps fail to develop. Implementing the 'sweep' AP with PM style 3 results in retinotopic maps that increase and then decrease in quality as the number of iterations increases (Fig.30). This AP in its current form does not yield viable retinotopic maps.

'Ocular dominance'

The left and right halves of the retinal sheet are alternately activated. This is designed to investigate how the two retinas compete for the tectum during development (the left and right halves of the retinal sheet in the model representing the retinas of the different eyes). The map fails to develop with PM style 1 (Fig.31A), this is likely a consequence of the over-correlated retinal acivity. With PM style 3, two distinct 'nodes' form on the left and right hand sides of the retinal sheet (Fig.31B), which in this example represent the centres of the left and right retinas. The 'nodes' fail to develop into proper maps as a consequence of over-correlation.

'Strobe'

The 'strobe' AP is hugely over-correlated; hence *a priori* the network is not expected to self-organise (Fig.32).

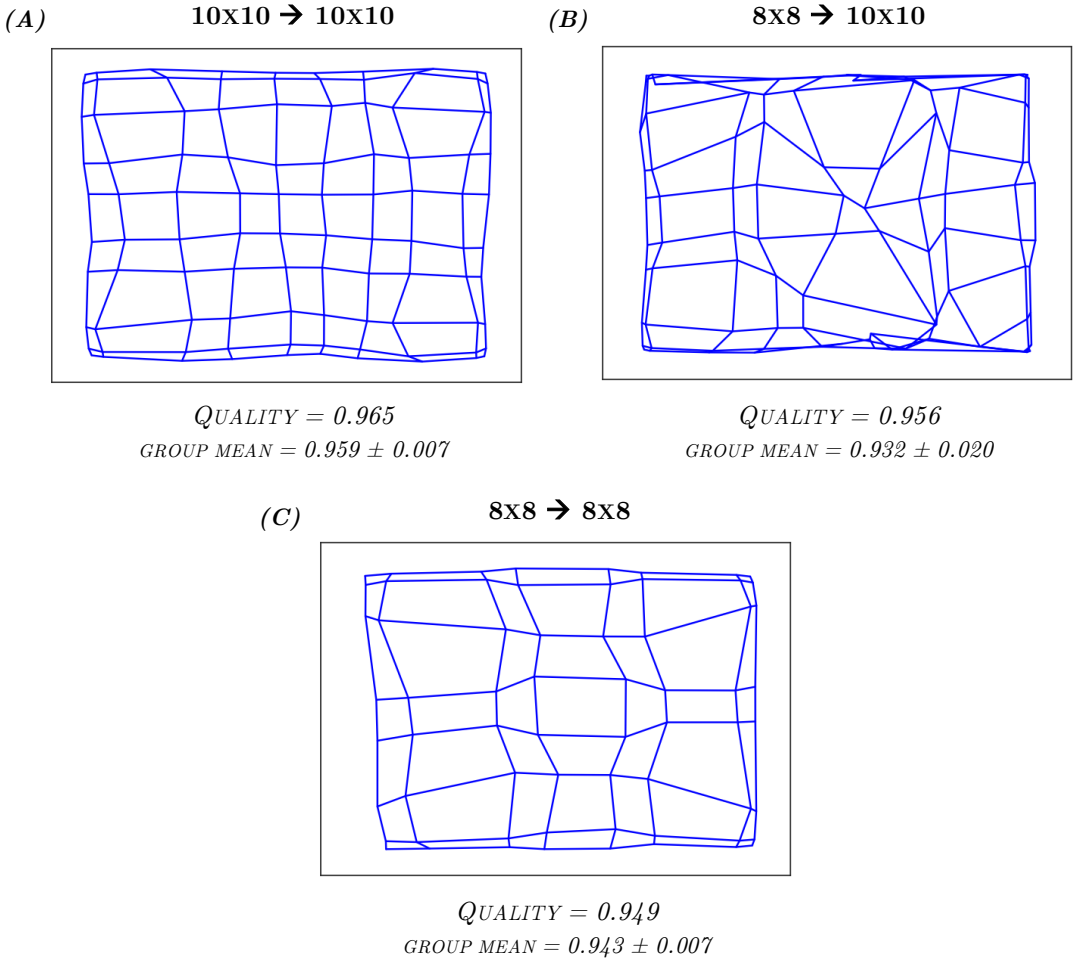

Figure 20: Plots demonstrating systems matching. All three plots were produced using PM style 1 and pairs AP. (A) 10x10 retinal sheet and 10x10 tectal sheet. (B) 8x8 retinal sheet and 10x10 tectal sheet. (C) 10x10 retinal sheet and 8x8 tectal sheet.

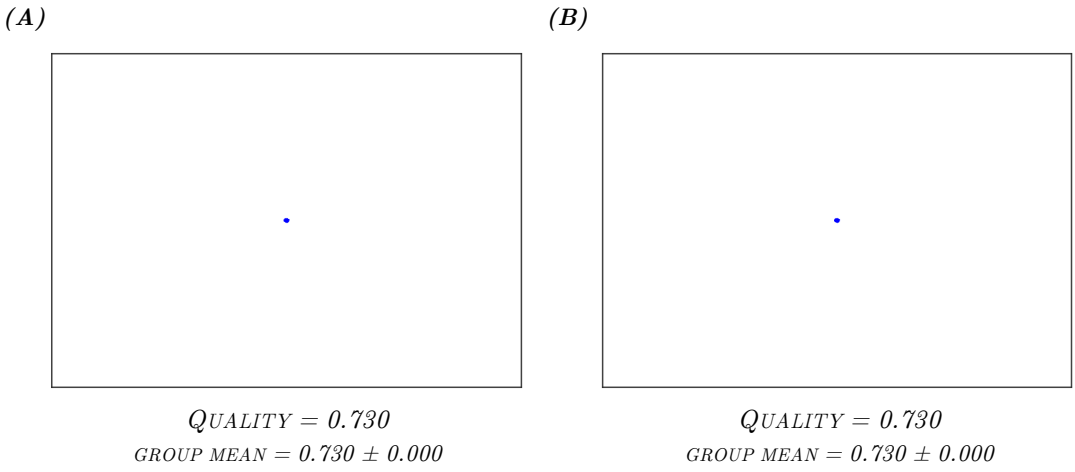

Figure 21: No polarity markers. Both plots use the 'pairs' AP. (A) 's' after 0 iterations. (B) 's' after 500,000 iterations.

(A) *(B)*

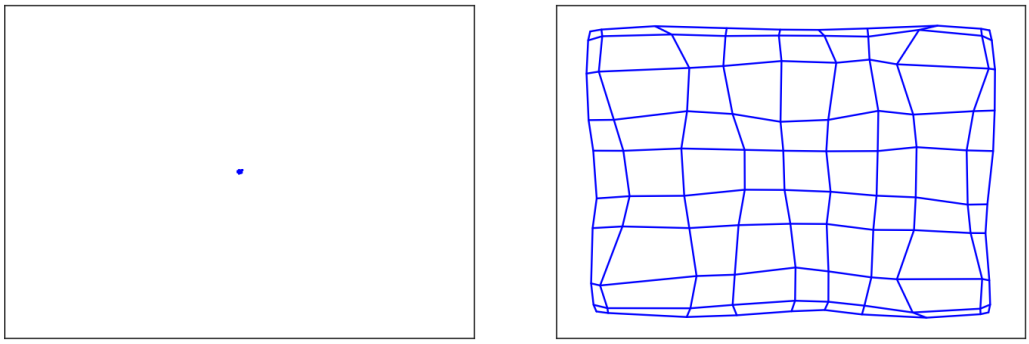

QUALITY = 0.731
GROUP MEAN = 0.731 ± 0.000

QUALITY = 0.965
GROUP MEAN = 0.959 ± 0.007

Figure 22: Style 1 polarity markers. Both plots use the 'pairs' AP. (A) 's' after 0 iterations. (B) 's' after 500,000 iterations.

(A) *(B)*

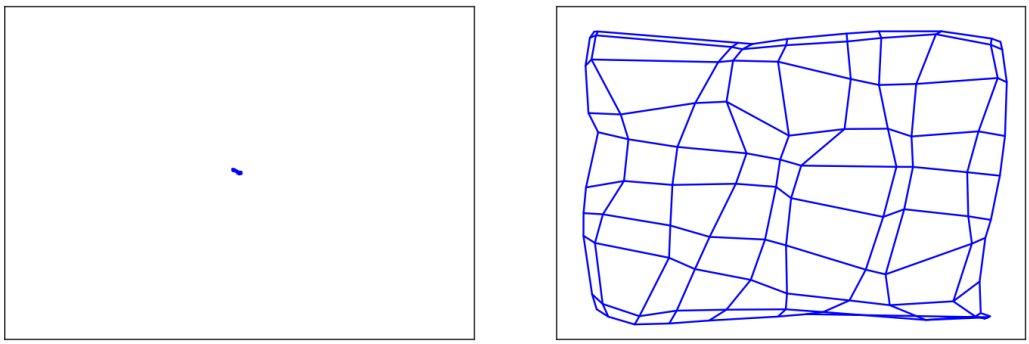

QUALITY = 0.730
GROUP MEAN = 0.730 ± 0.000

QUALITY = 0.952
GROUP MEAN = 0.750 ± 0.085

Figure 23: Style 2 polarity markers. Both plots use the pairs AP. (A) 's' after 0 iterations. (B) 's' after 500,000 iterations.

(A) *(B)*

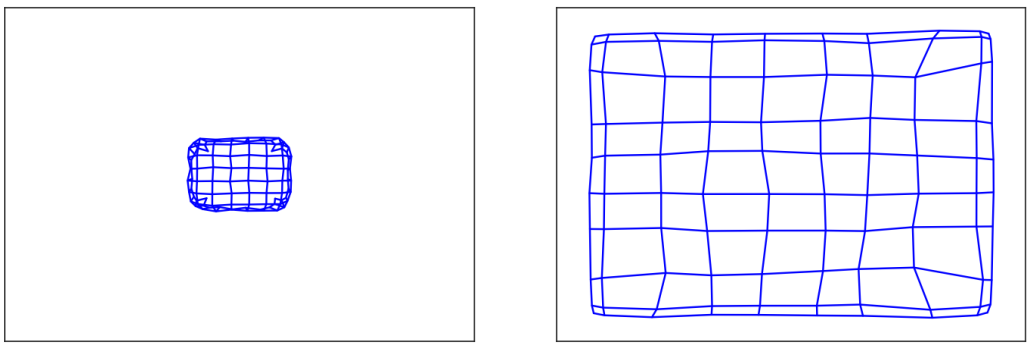

QUALITY = 0.797
GROUP MEAN = 0.797 ± 0.000

QUALITY = 0.975
GROUP MEAN = 0.976 ± 0.000

Figure 24: Style 3 polarity markers. Both plots use the pairs AP. (A) 's' after 0 loops. (B) 's' after 500,000 loops. The centres of mass of the corners of the embryonic retinotopic map introduced by style 3 fold over the rest of the map; this is a consequence of the way in which style 3 is implemented — the corner tectal neurons have their strength increased to their neighbouring retinal neurons on the inside of the sheet, but not to those on the outside, as they do not exist.

(A) *(B)*

Quality = 0.850
group mean = 0.832 ± 0.012

Quality = 0.854
group mean = 0.855 ± 0.001

Figure 25: Retinotopic maps produced using the 'two pairs' activity pattern. (A) Polarity marker style 1. (B) Polarity marker style 3.

(A) *(B)*

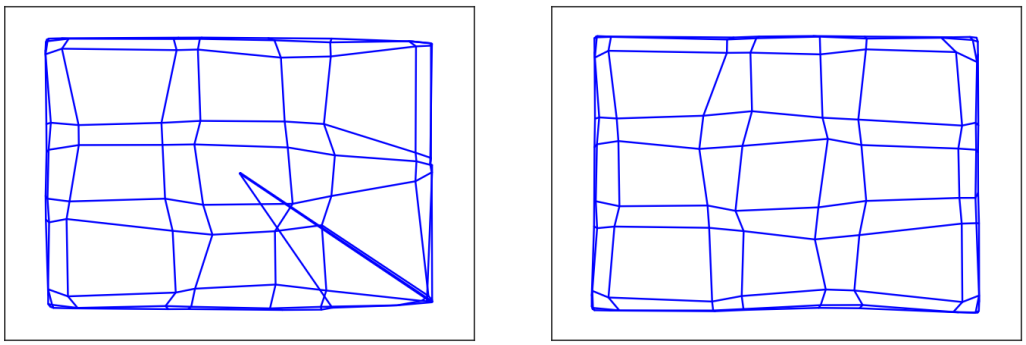

Quality = 0.941
group mean = 0.898 ± 0.026

Quality = 0.953
group mean = 0.953 ± 0.001

Figure 26: Retinotopic maps produced using the 'squares' activity pattern. (A) Polarity marker style 1. (B) Polarity marker style 3.

(A) *(B)*

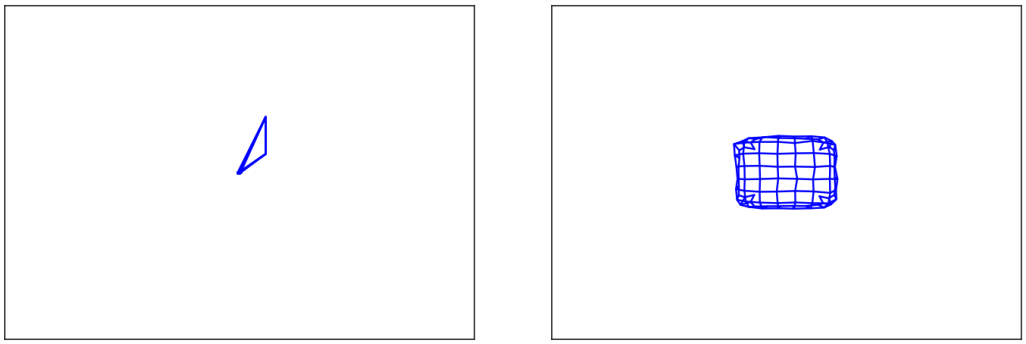

Quality = 0.736
group mean = 0.737 ± 0.004

Quality = 0.797
group mean = 0.797 ± 0.000

Figure 27: Retinotopic maps produced using the 'singles' activity pattern. (A) Polarity marker style 1. (B) Polarity marker style 3.

(A)

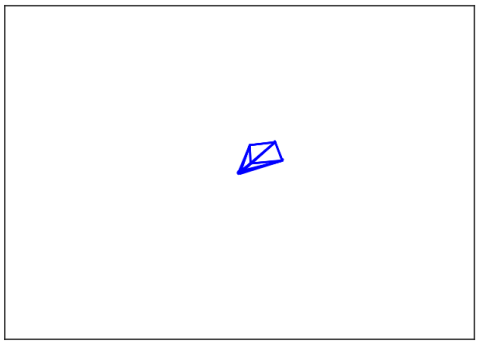

Quality = 0.744
group mean = 0.743 ± 0.001

(B)

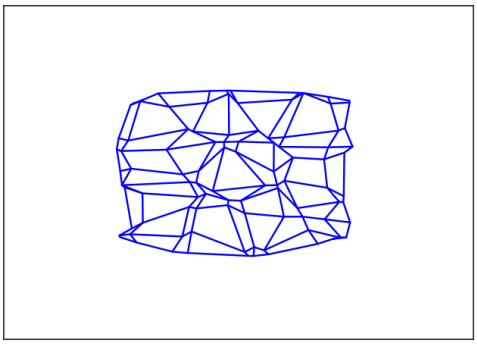

Quality = 0.860
group mean = 0.861 ± 0.002

Figure 28: Retinotopic maps produced using the 'two singles' activity pattern. (A) Polarity marker style 1. (B) Polarity marker style 3.

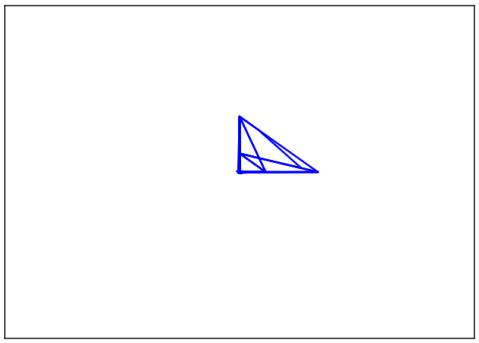

Quality = 0.741
group mean = 0.742 ± 0.000

Figure 29: Retinotopic map produced using the 'sweep' activity pattern and polarity marker style 1.

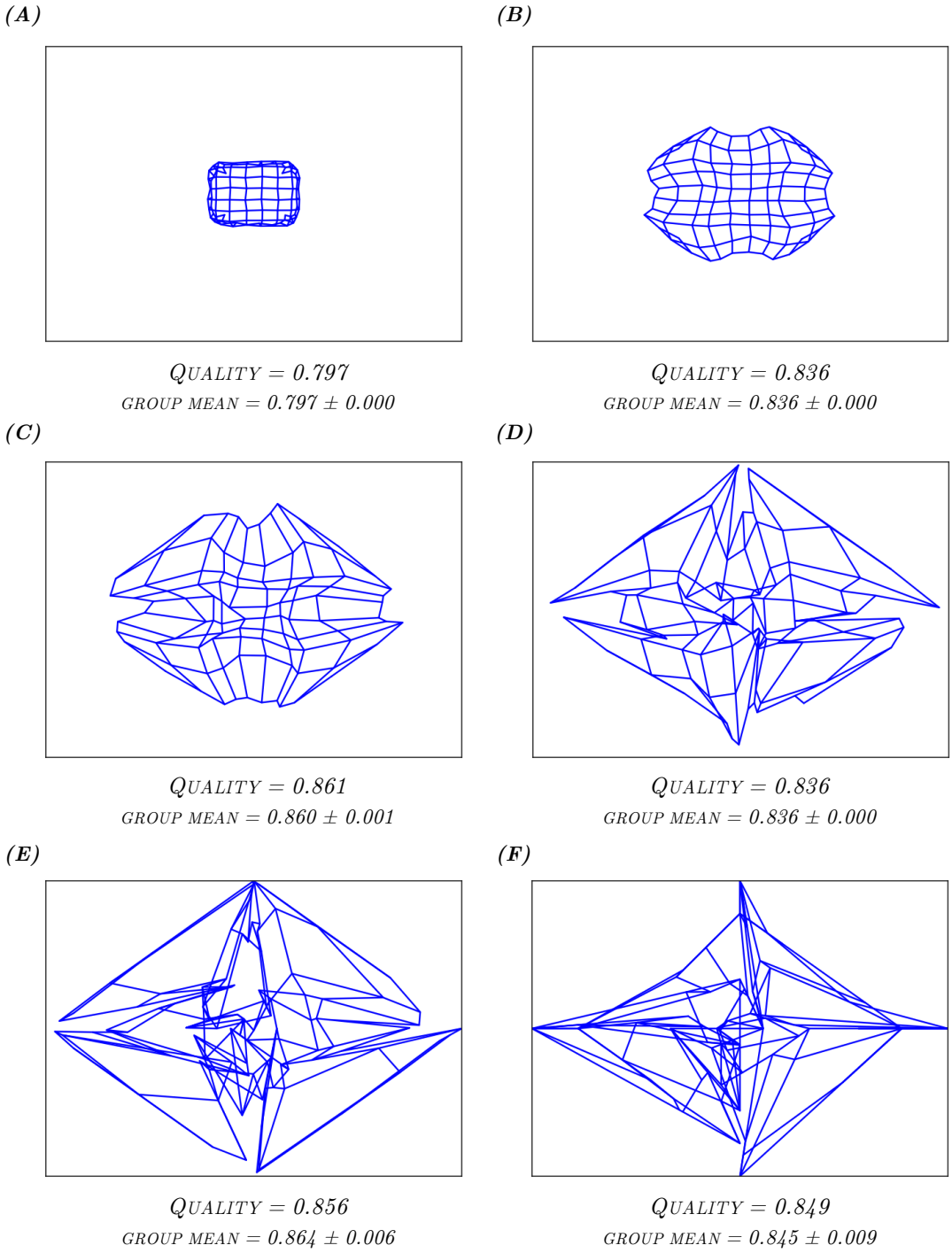

Figure 30: Retinotopic maps produced using the 'sweep' activity pattern and polarity marker style 3 after increasing numbers of iterations. (A) 0 iterations. (B) 12,500 iterations. (C) 25,000 iterations. (D) 50,000 iterations. (E) 100,000 iterations. (F) 500,000 iterations.

(A) *(B)*

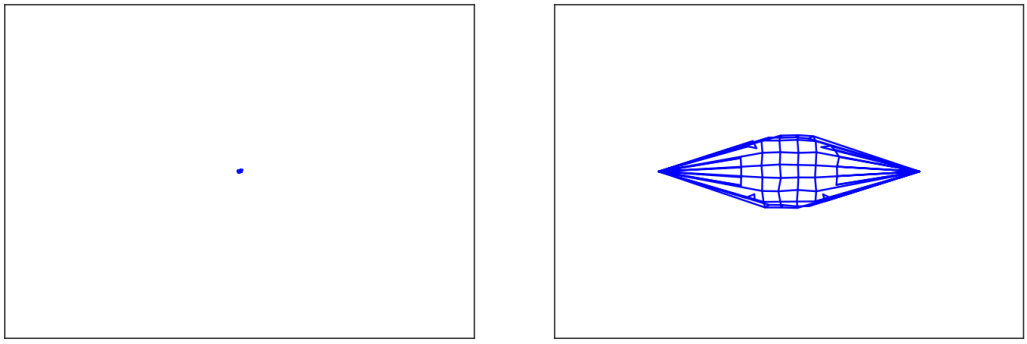

QUALITY = 0.731
GROUP MEAN = 0.731 ± 0.000

QUALITY = 0.808
GROUP MEAN = 0.808 ± 0.001

Figure 31: Retinotopic maps produced using the 'ocular dominance' activity pattern. (A) Polarity marker style 1. (B) Polarity marker style 3.

(A) *(B)*

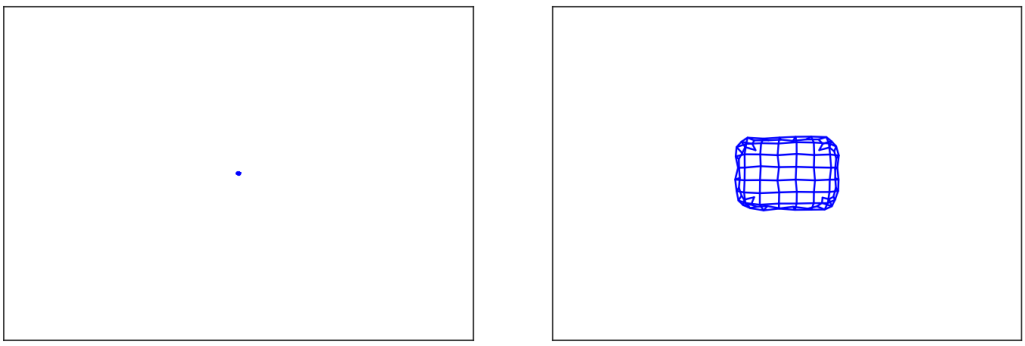

QUALITY = 0.730
GROUP MEAN = 0.730 ± 0.000

QUALITY = 0.797
GROUP MEAN = 0.797 ± 0.000

Figure 32: Retinotopic maps produced using the 'strobe' activity pattern. (A) Polarity marker style 1. (B) Polarity marker style 3.

DISCUSSION

Willshaw and Malsburg's neural activity theory of topographical network formation was evaluated by constructing a computational model in the Python™ programming language. This model was converted into the Cython programming language, which gives C-like performance to code predominantly written in Python™. This model was shown to be functionally robust by successfully replicating the original systems matching results from Willshaw and Malsburg, 1976.

Novel retinal activity patterns were developed and the model evaluated to investigate whether the neural activity theory is specific to the 'two pairs' AP used by Willshaw and Malsburg, or whether other retinal patterns with varying levels of correlation are also sufficient to induce network self-organisation.

A novel function was devised allowing retinotopic maps formed by the model to be assessed quantitatively. It was shown that retinotopic maps can form under the input from various different retinal APs. A discussion of what conclusions can be drawn from the results produced by the model, and the biological relevance, follows below. This is first preceded by a discussion of the advantages and constraints of the model used in this study.

THE MODEL: ADVANTAGES AND CONSTRAINTS

A key problem with the 6x6 retinal and tectal sheets predominantly used by Willshaw and Malsburg is that the direct impact of boundary effects affect all but one tectal neuron (the central one); the depolarisation of this neuron will also almost certainly be influenced by secondary effects of the boundaries. Boundary affects result from the asymmetric tectal interactions that occur at the edges of the tectal sheet reducing the overall depolarisation of these neurons. Increasing the speed of the model using Cython conferred two major advantages:

(1) Larger retinotopic maps could be produced, reducing the impacts of boundary effects

(2) Maps could be produced in batches, allowing mean and standard deviations in quality to be calculated

However, even using Cython the script still takes c.5 hours to run a batch of ten maps using 10x10 neural sheets and 500,000 iterations. The time taken to run the model increases supralinearly with increasing neural sheet sizes because the convergence stage of each iteration takes much longer. These computational constraints placed a limit on the size of the networks that could be modeled.

A second constraint is how map qualities are calculated. Currently the displacement of the synaptic centre of mass of a tectal neuron from its ideal location in the retinal sheet is normalized to the maximum possible displacement, e.g. the diagonal of the retinal sheet. This results in maps, even those that are qualitatively poor, having high qualities distributed within a narrow range (c.0.7-1.0). See FUTURE DIRECTIONS for ideas on how to improve this.

Producing maps with the same input parameters in batches and conducting descriptive statistics, has increased the reliability of the model output in an effort to combat the increasingly acknowledged replication crisis (Stodden et al., 2016).

CONCLUSIONS FROM NOVEL ACTIVITY PATTERNS

The maps produced using APs 'pairs', 'two pairs', 'squares' and 'two singles' all developed to some extent (Figures 20A, 25, 26 and 28). These results indicate that as long as there is some degree of correlation in retinal activity the network is able to self-organise. There are, however, caveats to this:

(1) If retinal activity is correlated across a large proportion of the retinal sheet (over-correlated activity), e.g. in the 'sweep', 'ocular dominance' and 'strobe' APs, then the tectal sheet cannot distinguish between the retinal neurons active at any one time. This tends to prevent maps forming to high qualities (Figures 29, 30, 31 and 32).

(2) Neurons at the boundaries of the tectal sheets fail to fully develop, with the centres of their receptive fields remaining close to those one layer inside.

(3) Maps formed using activity patterns with varying levels of retinal correlation (e.g. 'two pairs' and 'two singles') become well organized but are too small (Figures 25 and 28).

(4) Maps can fail to form using PM style 1; they tend to form to higher qualities, with lower variance, when PM style 3 is used.

Biological Relevance

Whilst trialing different APs, and different PM styles, on 10x10 neural grids is interesting from a theoretical standpoint — as it demonstrates that the neural activity model is functionally viable — it is important to consider what these results mean in the context of the significantly larger biological retino-tectal networks (the human optic nerve contains 1.7m axons) (Jonas et al., 1992). Important points to consider in the larger biological systems are:

(1) Boundary effects can essentially be ignored. The 10x10 retinal and tectal sheets modeled in this study are sufficiently large to demonstrate that away from the boundaries the maps form well. In a much larger network, a smaller proportion of the neurons will be affected by boundary effects, therefore allowing them to be disregarded. It is possible that another mechanism, such as marker-induction (Willshaw and Malsburg, 1979), acts to reduce the impact of boundary effects on the outermost layer of tectal neurons, or perhaps network wiring in higher brain areas is able to negate the effects of their skewed receptive fields.

(2) PM style 3 is biologically viable. In goldfish exposed to stroboscopic light conditions during optic nerve redevelopment, rough retinotopic maps still form (Eisele and Schmidt, 1988). This implies that a secondary mechanism for network organization is taking place alongside the neural activity model. Regardless of the mechanism responsible, introducing an embryonic schematic for retinotopic map formation using PM style 3 is biologically feasible as a consequence.

Maps produced using PM style 3 develop to a higher quality, with smaller deviations in quality, than those produced using PM style 1.

(3) Over-correlated retinal activity is less likely to be an issue in the much larger biological retinas. As the retinal sheet is so much larger, many more adjacent neurons can be active without impacting map formation, especially if a secondary mechanism is also acting to organize the network. The 'sweep' AP is based on retinal activity observed in neonatal mammals (Galli and Maffei, 1988; Maffei and Galli-Resta, 1990; Meister et al., 1991; Wong et al., 1993). *In vivo*, the waves of retinal activity do not span the entire sheet, nor do they only travel in rigid lines parallel to the edges of the sheet. Some form of network organization occurs with the simplistic 'sweep' AP modeled in this study (Fig.30). Further modeling could be used to investigate whether larger maps, with smaller areas of active retinal neurons, moving in more variable directions, increases the quality of the maps formed.

(4) The 'ocular dominance' AP demonstrates that overly correlated activity in the two retinas can lead to differentiation in the areas of the tectum that their afferents occupy (Fig.31). However the tectum of fish and amphibians is divided into many small ocular dominance columns (Boss and Schmidt, 1984). In a much larger retina it is possible that highly correlated retinal activity in comparatively smaller areas of each retina could lead to the differentiation of retinal afferents into the aforementioned ocular dominance columns. Tetrodotoxin injections reduce the formation of ocular dominance columns in fish, implying that neural activity is responsible for their formation (Boss and Schmidt, 1984).

Limitations of the Neural Activity Model

The neural activity model is unable to account for the results observed in tectal rotation experiments (Yoon, 1973). A section of the tectum is dissected out, rotated 180° and reimplanted. The visual projection from the retina to the section of reimplanted tectum was shown to be organised in a completely reverse retinotopic order compared to the surrounding tectum. This indicates that the reimplanted tectum retains its original topographic polarity regardless of whether it is rotated or not, e.g. the tectal neurons 'remember' which retinal axons they originally synapsed with, implying a marker mechanism.

Future Directions

Converting the model to the C programming language would further reduce run-time, allowing the modeling of larger networks. A larger network would allow the modeling of a more realistic 'sweep' activity pattern. Furthermore, a faster model would allow more iterations to be conducted. As discussed above, APs with varying correlations ('two pairs' and 'two singles') tend to produce retinotopic maps with the correct relative positions of the tectal neurons, but that are too small (Figures 25 and 28 respectively). There are two potential explanations for this:

(1) The map is underdeveloped and a larger map could be obtained with more iterations

(2) The map cannot develop to be larger. The correlated retinal activity acts to develop specific retino-tectal connections, therefore expanding the map, while the uncorrelated activity acts to develop diffuse retino-tectal connections, thus shrinking the map. The relative probability of these two types of activity occurring sets the limit on the size to which maps can develop.

By increasing the number of iterations these two theories can be differentiated between. If it is (1), this is an interesting development; intuitively the inherent stochasticity of neural networks would tend to result in some degree of uncorrelated

activity — if networks are able to self-organise in the face of seemingly uncorrelated activity it implies that the neural activity model is highly robust.

Concluding Remarks

The neural activity model of topographic map formation is able to explain the self-organisation of neural networks. It is able to account for systems matching properties and is robust to various different retinal activity patterns. Further research requires the conversion of the model into a faster programming language (e.g. C) and should focus on larger networks and biologically observed activity patterns. The model is unable to account for tectal rotation experiments, implying that both neural activity and marker mechanisms play a role in network development *in vivo*.

***

Acknowledgments

I would like to thank my supervisor, Dr. Stephen Eglen, for his support, guidance and patience; without his help this project would not have come to fruition. I would also like to thank Professor David Willshaw, whose personal correspondence helped me to spot an error in the code that was preventing retinotopic map formation, saving crucial time. Finally, I would like to thank the staff of the St. John's College library for providing me with a quiet space in which to build the model and construct this report.

References

Apter, J.T. (1945). Projection of the retina on superior colliculus of cats. J. Neurophysiol. *8*, 123–134.

Arroyo, D.A., and Feller, M.B. (2016). Spatiotemporal Features of Retinal Waves Instruct the Wiring of the Visual Circuitry. Front. Neural Circuits *10*.

Boss, V.C., and Schmidt, J.T. (1984). Activity and the formation of ocular dominance patches in dually innervated tectum of goldfish. J. Neurosci. Off. J. Soc. Neurosci. *4*, 2891–2905.

Cooper, S., Daniel, P.M., and Whitteridge, D. (1953). Nerve impulses in the brainstem of the goat. Short latency responses obtained by stretching the extrinsic eye muscles and the jaw muscles. J. Physiol. *120*, 471–490.1.

Eisele, L.E., and Schmidt, J.T. (1988). Activity sharpens the regenerating retinotectal projection in goldfish: sensitive period for strobe illumination and lack of effect on synaptogenesis and on ganglion cell receptive field properties. J. Neurobiol. *19*, 395–411.

Galli, L., and Maffei, L. (1988). Spontaneous impulse activity of rat retinal ganglion cells in prenatal life. Science *242*, 90–92.

Gaze, R.M. (1958). The Representation of the Retina on the Optic Lobe of the Frog. Q. J. Exp. Physiol. Cogn. Med. Sci. *43*, 209–214.

Gaze, R.M., and Keating, M.J. (1972). The Visual System and "Neuronal Specificity''. Nature *237*, 375–378.

Gaze, R.M., Keating, M.J., Szekely, G., and Beazley, L. (1970). Binocular Interaction in the Formation of Specific Intertectal Neuronal Connexions. Proc. R. Soc. Lond. B Biol. Sci. *175*, 107–147.

Goodhill, G.J. (1993). Topography and ocular dominance: a model exploring positive correlations. Biol. Cybern. *69*, 109–118.

Hebb, D.O. (1949). The organization of behavior; a neuropsychological theory (Oxford, England: Wiley).

Jonas, J.B., Schmidt, A.M., Müller-Bergh, J.A., Schlötzer-Schrehardt, U.M., and Naumann, G.O. (1992). Human optic nerve fiber count and optic disc size. Invest. Ophthalmol. Vis. Sci. *33*, 2012–2018.

Maffei, L., and Galli-Resta, L. (1990). Correlation in the discharges of neighboring rat retinal ganglion cells during prenatal life. Proc. Natl. Acad. Sci. *87*, 2861–2864.

McNaughton, B.L., Battaglia, F.P., Jensen, O., Moser, E.I., and Moser, M.-B. (2006). Path integration and the neural basis of the "cognitive map." Nat. Rev. Neurosci. *7*, 663–678.

Meister, M., Wong, R.O.L., Baylor, D.A., and Shatz, C.J. (1991). Synchronous bursts of action potentials in ganglion cells of the developing mammalian retina. Science *252*, 939–944.

Moser, E.I., Roudi, Y., Witter, M.P., Kentros, C., Bonhoeffer, T., and Moser, M.-B. (2014). Grid cells and cortical representation. Nat. Rev. Neurosci. *15*, 466–481.

Penfield, W., and Boldrey, E. (1937). Somatic motor and sensory representation in the cerebral cortex of man as studied by electrical stimulation. Brain J. Neurol. *60*, 389–443.

Prestige, M.C., and Willshaw, D.J. (1975). On a Role for Competition in the Formation of Patterned Neural Connexions. Proc. R. Soc. Lond. Ser. B *190*, 77–98.

Rose, J.E., Galambos, R., and Hughes, J.R. (1959). Microelectrode studies of the cochlear nuclei of the cat. Bull. Johns Hopkins Hosp. *104*, 211–251.

Sperry, R.W. (1943). Visuomotor coordination in the newt (triturus viridescens) after regeneration of the optic nerve. J. Comp. Neurol. *79*, 33–55.

Sperry, R.W. (1963). Chemoaffinity in the orderly growth of nerve fiber patterns and connections. Proc. Natl. Acad. Sci. U. S. A. *50*, 703–710.

Stodden, V., McNutt, M., Bailey, D.H., Deelman, E., Gil, Y., Hanson, B., Heroux, M.A., Ioannidis, J.P.A., and Taufer, M. (2016). Enhancing reproducibility for computational methods. Science *354*, 1240–1241.

Talbot, S.A., and Marshall, W.H. (1941). Physiological Studies on Neural Mechanisms of Visual Localization and Discrimination. Am. J. Ophthalmol. *24*, 1255–1264.

Willshaw, D.J., and Malsburg, C.V.D. (1976). How Patterned Neural Connections Can Be Set Up by Self-Organization. Proc. R. Soc. Lond. B Biol. Sci. *194*, 431–445.

Willshaw, D.J., and Malsburg, C.V.D. (1979). A Marker Induction Mechanism for the Establishment of Ordered Neural Mappings: Its Application to the Retinotectal Problem. Philos. Trans. R. Soc. Lond. B Biol. Sci. *287*, 203–243.

Wong, R.O.L., Meister, M., and Shatz, C.J. (1993). Transient period of correlated bursting activity during development of the mammalian retina. Neuron *11*, 923–938.

Woolsey, C.N. (1952). Patterns of localization in sensory and motor areas of the cerebral cortex. Biol. Ment. Health Dis. 193–206.

Yoon, M.G. (1973). Retention of the original topographic polarity by the 180° rotated tectal reimplant in young adult goldfish. J. Physiol. *233*, 575–588.2.

Appendix

The appendix of this study contains the appendix of Willshaw and Malsburg, 1976. It is referenced heavily in Material and Methods.

Here is a description of the calculations performed on the computer.

The strength of the synaptic connection between cell i in a sheet of M presynaptic cells and cell j in a sheet of N postsynaptic cells is specified by the entry s_{ij} in the $M \times N$ matrix s. The activity H_j^* in postsynaptic cell j is determined by its membrane depolarization H_j, and is calculated according to a linear threshold model of a nerve cell (Malsburg 1973). At time t, cell j is deemed to fire if its depolarization exceeds a fixed threshold value θ. Its activity $H_j^*(t)$ is defined as

$$H_j^*(t) = \begin{cases} H_j(t) - \theta & \text{if} \quad H_j(t) > \theta, \\ 0 & \text{otherwise.} \end{cases}$$

To calculate the membrane depolarization we assume that its rate of change $\partial H_j / \partial t$ is proportional to the sum of the excitatory effects of active presynaptic cells, the excitation and inhibition supplied by nearby active postsynaptic cells and a decay term due to losses in the membrane itself. It is helpful to define the quantities $A_i^*(t)$, e_{kj} and i_{kj}. The variable $A_i^*(t)$, used to describe the state of the presynaptic cells, has value 1 if cell i is active at time t and 0 otherwise. The time independent parameters e_{kj} and i_{kj} specify the short range excitation and inhibition exerted by postsynaptic cell k on postsynaptic cell j.

We can then write a set of N coupled equations.

$$\frac{\partial H_j(t)}{\partial t} + \alpha H_j(t) = \sum_i A_i^*(t)\, s_{ij}(t) + \sum_k H_k^*(t)\, e_{kj} - \sum_k H_k^*(t)\, i_{kj} \quad \text{for} \quad j = 1,2,3,\ldots, N.$$

The first sum represents the contributions from the presynaptic cells; the other two are the excitatory and inhibitory contributions from the postsynaptic cells. The parameter α is the membrane time constant. To ensure that cells which do not mark polarity have initially no particular preference for any cell in the opposite sheet, all initial values of the entries in s are chosen from a set of random numbers normally distributed about a positive mean. The numbers are then adjusted to give synapses between polarity marker cells above-average strengths. The following procedures are carried out for each successive trial, during which the postsynaptic cells are stimulated by a given set of presynaptic cells.

(1) A small cluster of c presynaptic cells is chosen at random from the whole set of overlapping clusters of that size covering the presynaptic sheet. These cells constitute the input to the postsynaptic sheet during this trial. (This is where we assume that dispersed patterns of activity that can also occur have no significant effect.)

(2) For each of the N postsynaptic cells a stationary solution for its membrane depolarization is found by iterating the set of coupled equations until the mean change in depolarization per unit of time becomes less than 0.5 %.

(3) Only those synapses between cells firing sufficiently strongly are strengthened. The increase in strength Δs_{ij} of synapse s_{ij} is given by

$$\Delta s_{ij} = h A_i^* H_j^*$$

Figure 33: First page of the Willshaw and Malsburg, 1976, appendix

provided that H_j^*, as calculated in step 2, exceeds the modification threshold ϵ, and where the constant h sets the speed of organization.

(4) The synaptic strengths are then renormalized so as to keep the mean strength associated with each postsynaptic cell at a constant value S, thus

$$\frac{1}{M}\sum_{i=1}^{M} s_{ij} = S \quad \text{for} \quad j = 1, 2, \ldots, N.$$

The parameters $c, \alpha, \theta, h, \epsilon, S$ and the entries in the matrices i and e are constants, whose values have to be found by trial and error. The values used in the main body of calculations were

$$c = 2, \quad \theta = 10.0, \quad \alpha = 0.5, \quad h = 0.016, \quad \epsilon = 2.0, \quad S = 2.50.$$

A postsynaptic cell could influence other postsynaptic cells up to a distance 3 units away, the distance between the two cells with coordinates (x, y) and (x', y') being defined as the sum $|x-x'|+|y-y'|$. The postsynaptic excitatory and inhibitory constants took the following values

distance between cells j and k	1	2	3
e_{kj}	0.05	0.025	—
i_{kj}	—	—	0.06

For the initial values in the matrix s a set of MN random numbers were first chosen from a normal distribution of mean 2.50 and standard deviation 0.14. The values of the entries designating synapses between polarity markers were then increased fivefold, and then all the numbers were normalized, as in step (4) given above.

For the extra simulation to investigate the disruptive effect of dispersed presynaptic activity, the stimuli used were chosen equiprobably from the set of 1800 pairs of pairs of neighbours which can be formed from the members of a 6×6 sheet. Under these conditions, four instead of two presynaptic cells were active per trial, and to cater for this θ and ϵ were doubled, to take the values 20.0 and 4.0, and h was decreased to 0.005. All other parameters retained the values given above.

Figure 34: Second page of the Willshaw and Malsburg, 1976, appendix.